JOURNAL OF MATERIALS SCIENCE **38** (2003) 2875–2881

A preliminary study on laser assisted aluminum foaming

Y. P. KATHURIA*
Department of Robotics, Faculty of Science and Engineering, Ritsumeikan University, Kusatsu-shi Shiga-ken 525-8577, Japan
E-mail: ykv21024@se.ritsumei.ac.jp

Closed cell cellular solids defined by randomly distributed air pores in metallic matrix are a special class of light weight porous material that exhibit several unique characteristic applications in various domains of industries. Among these, in particular aluminum foam has shown a popular interest in recent years and is potentially used for many applications due to its light weight structure. In this paper laser assisted foaming experiments have been performed using CO_2/Nd-YAG lasers. The results show a unidirectional and localized expansion of foam. Closed cell porous aluminum structures with different relative densities (0.39–0.33) and porosity of (61–67%) are fabricated. It is found that the beam interaction time ($t_{\text{int.}}$ = spot size/processing speed), the so called dwell time, plays a significant role in the evolution of the cell morphology and the expansion mechanism of foam. Preliminary results suggest that a pore size gradient and a density gradient exist in the structure as the processing condition changes. The foam has large pores and lower density for slow processing speed, in contrast to the fast processing speed with small pore size but higher density. Additionally, a few examples on laser assisted cutting of aluminum foam are also well demonstrated. © *2003 Kluwer Academic Publishers*

1. Introduction

Recently there has been growing interest in metal foaming and net-shaping [1–27]. They combine the advantages of a metal with the structural advantages of foam. Among these, aluminum foam have created a special interest due to its light weight structure and its various applications in the automotive, aerospace and allied industries. Besides that advances in the near net-shaping of the aluminum foam have expanded the possibilities in the structural applications [20]. For example, tailored blanks with foamable aluminum sandwich material offer the possibility of structural parts for car bodies. But the manufacturing techniques and characterization methods need more attention for their effective and economical use in the industries. Various methods [2–5] including the casting and powder metallurgy techniques have been used that employ the conventional melting and molding process to produce aluminum foam and hence a near net-shape structure. Here an alternative process of using laser as a heat source shall be described. It has an inherent advantage of unidirectional and localized foaming. Besides that the process is much faster, due to the rapid solidification process, where the stabilization of pore formation could partly be controlled by coaxial gas flow and the laser processing parameters. In the present paper, based upon powder metallurgy (P/M) and laser heating process, it is demonstrated that this unidirectional and localized expansion of the aluminum foam using the Nd-YAG/CO_2 laser is feasible. Though the experimental study was done using both the lasers, but the detail study was carried out using the CO_2-laser only. Thereby the basic process of beam interaction time with the foamable precursor material is investigated. In addition, an examination is made of the influence of the processing conditions on the evolution of cell morphology, and results concerning the density gradient are interpreted. The combination of such an approach will allow us to study the physical aspects of laser assisted foaming with respect to its production and quality.

2. Laser assisted foaming

The basic principle of laser assisted foaming is shown schematically in Fig. 1. It is produced by mixing powdered material and a foaming agent and subsequently cold isostatic pressing the mixture to a foamable sandwich precursor material [3]. The material is foamed by heating it up to its melting point by a high power laser beam irradiation. The unidirectional expansion of the foamable precursor material can be observed during the entire foaming process in the irradiation direction. The

*Formerly at: Laser X Co. Ltd., Chiryu-shi Aichi-ken, Japan.

Part of this work was presented at TMS/ASM-2000 annual meeting (Oct.10–13, 2000) in St. Louis, USA and also in Euromat-2001 (June 10–14, 2001) in Rimini, Italy.

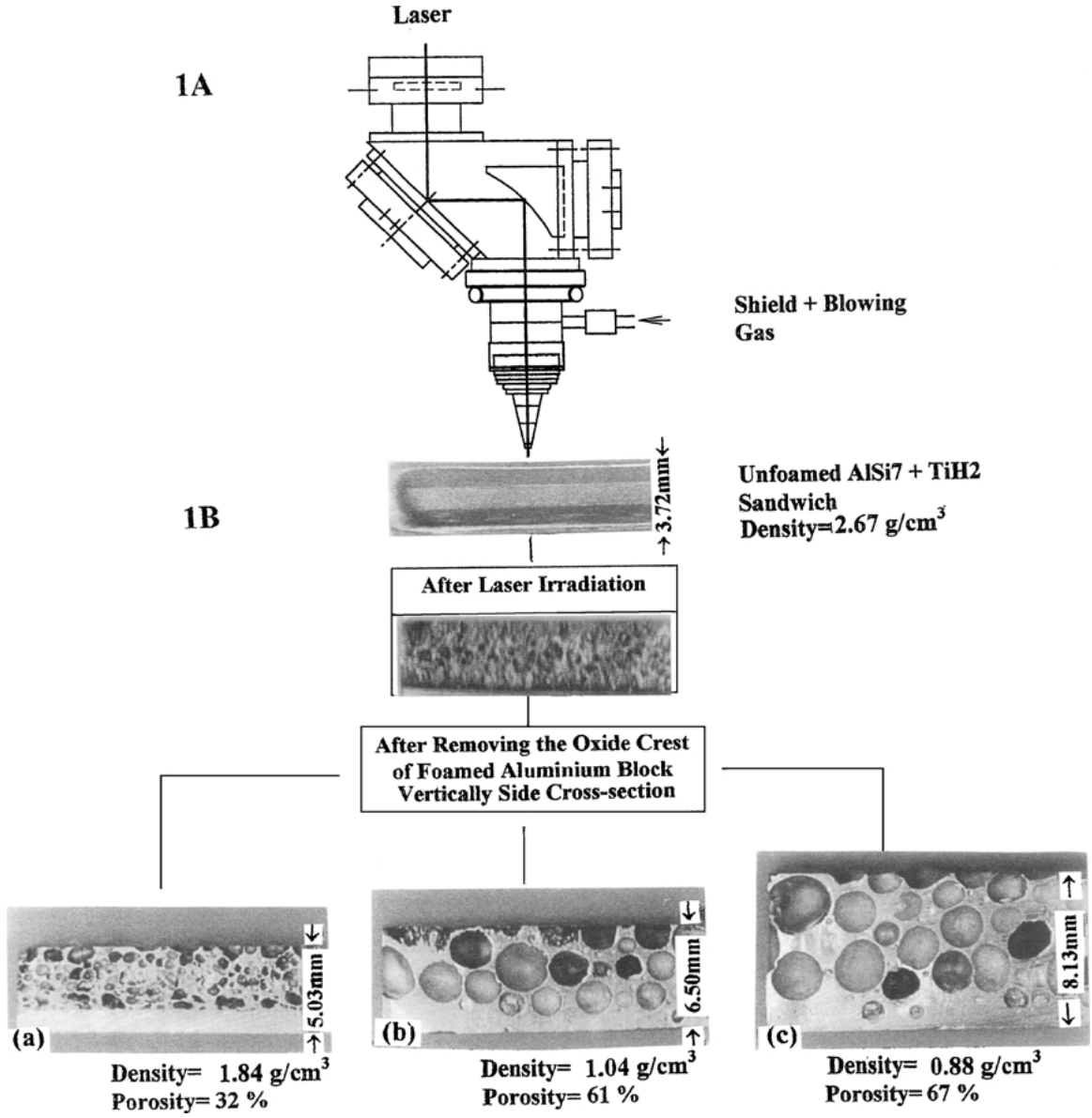

Figure 1 Photographic view (A) and vertically side cross-section (B) of Al-foam. Laser: cw CO_2. Processing parameters: $P = 5$ kW; $Ar = 30$ l/min; Processing speed (V) = (B-a): 2 m/min; (B-b): 0.8 m/min; (B-c): 0.4 m/min.

expansion in the other directions is negligibly small. Previous work [10] recognised that the laser beam interaction time ($t_{\text{int.}}$ = spot size/processing speed), the so called dwell time, plays a significant role in the evolution of the cell morphology and the expansion mechanism of foam. Analysis showed that, in a narrow range of power density and beam interaction time, coupled with cooling rate and extent of porosity, the build-up foamed structure span the entire region, although most of the useful working points lie on the diagonal line in Fig. 2. Besides this, the foaming characteristics change continuously as one moves from the short interaction time region (marked A in Fig. 2) to the long interaction time region (marked C in Fig. 2) along the diagonal line.

In the aluminum foaming process, first an aluminum sandwich with aluminum foam core is produced. This can be done by mixing aluminum alloy powder (Al-7%Si) with a fraction of foaming agent (0.5%TiH_2). Its typical particle size being 40 μm. Ca and Mg can be added to increase viscosity and decrease surface

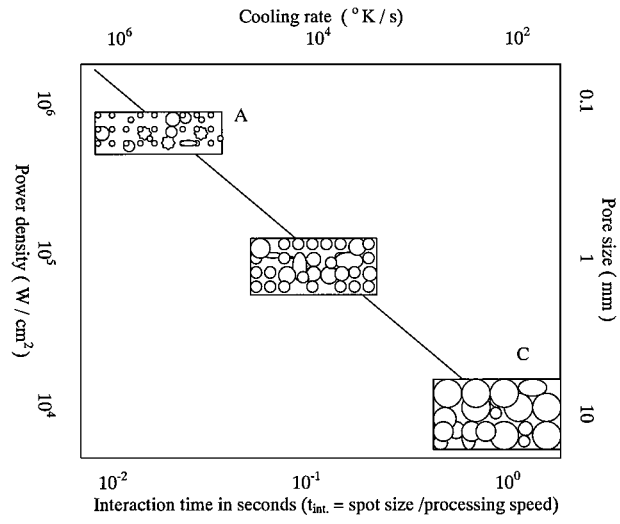

Figure 2 Block diagram of build-up foamed structure versus processing conditions for laser assisted foaming.

tension. The powder mixture is then compressed to the extrusion billets by cold isostatic press (CiP), which is about 80% in density. The CiP expandable billets are then extruded between two covering sheets of non-expandable aluminum to a 100% dense material. During the deformation process under pressure, a metallic bond is created between the material of the covering sheet and the extrusions. The laser irradiation heats up this Al-alloy sandwich above its melting point of 660°C and thereby the foaming agent TiH_2 expands the material. It is believed that at high temperature, the foaming agent titanium hydride decomposes into titanium and hydrogen gas. Titanium released from the foaming agent remains in the aluminum and perhaps precipitates as intermetallic compound $TiAl_3$ [6], whereas the hydrogen gas released, tends to bubbles out, causing the melt to expand thus resulting in the bubble formation. These gas bubbles are free to move around and tend to a state of lowest surface energy, while the liquid accumulates at the edges of the bubbles, forming the final structure as macroscale porosity [7]. However, a fraction of the gas still remains trapped inside the solidified foam, due to its 20-times solubility difference in liquid and solid aluminum and thus accounts for the microscale porosity. The blowing or shield gas Ar used is an additional help for the formation of the porosity may also become trapped inside the solidified foam. In the conventional thermal melting process, the average temperature gradient of the interface that varies as the bulk temperature is lower. This is accompanied by a slow cooling rate and hence long time for the stabilization of the pores to occur. On the other hand in the case of laser process the average temperature gradient of the interface is much higher thus faster cooling rate and hence the pore stabilization. The figure also illustrate, as to how the processing speed could affect the cell morphology and the expansion ratio of the build-up foam.

3. Experimental procedure

The experiments were performed in three steps. In the first part, laser foaming experiments were carried out with a 5 kW cw CO_2-laser beam. This is focused further by a ten-inch focal length off-axis parabolic mirror onto the target surface. The working distance was varied to produce a defocused spot size of 2–10 mm onto the test piece. An argon gas jet, with a flow rate of 20–40 l/min, and coaxial to the beam axis, was used to shield the melt pool from oxidation. In the case of foaming, the same gas was also used as the blowing gas. The foamable but unfoamed Al-alloy sandwich sample of size ($15 \times 15 \times 0.4$ cm), was procured from Fraunhofer Institute (IFAM) Bremen and fabricated according to the P/M (Powder Metallurgy) procedure described elsewhere [2, 3]. This was further cut into several test pieces of dimension $50 \times 14 \times 4$ mm respectively. Due to highly reflective surface, they were made rough by emery paper or by the sand blasting technique and finally black spray coated, to increase the absorption of laser radiation. Foaming was accomplished by irradiating the substrate test piece under the stationary laser beam. The substrate was moved under the beam by the numeric XY-table. The essential parameters to generate the desired porosities for foamed structure are given in the Table Ia. To study a different level of porosity, the foaming tracks were made for various processing speeds. A few of the test samples generated with this technique are shown in Fig. 1 respectively, whereas the Fig. 3 shows the corresponding pictorial view of these porous structures.

TABLE I Processing parameters

1a: CO_2-Laser	1b: Nd-YAG Laser
Power (P): 3.0–5.0 kW	$P_{avg} = 2$ kW
Spot size: 2.0–10.0 mm	$P_{peak} = 4$ kW
Processing speed (V):	Duty cycle = 50%
0.4–2.0 m/min	Pulse repetition rate = 100 Hz
Ar gas flow rate: 20–40 l/min	Processing speed = 0.3–0.5 m/min
Pressure: 2.5 kg/cm^2	Shield gas (Ar) = 50 l/min

In the second part, similar experiments were repeated with a multiwave Nd-YAG laser. Compared to CO_2-laser radiation, aluminum exhibits higher absorption at wavelength (λ) = 1.06 μm (Nd-YAG). Therefore, it is anticipated that relatively better beam coupling efficiency could yield faster evolution of the foam. The power of the Nd-YAG laser (Lumonics Model: MW2000) used can be varied from cw to high energy pulsed mode with sine and square wave modulation functions. The incident angle of the laser beam was set at 10 degrees to the normal surface. This is to prevent the reflections from the target back towards the laser oscillator. Besides that, the absorption of the laser beam shows a maximum close to this position. The pre-preparation of the substrate test piece was done as described above. In this case the beam was just focussed onto the target surface. The spot size of the beam is of the order of 500 μm. The foaming tracks were made for various processing parameters e.g., laser power, duty cycle and processing speed etc., but the optimum results of the generated foam structure were obtained with the parameters given in Table Ib. Fig. 4 shows a few of the test samples produced by using this procedure.

The nominal chemical composition of the unfoamed Al-alloy sandwich used is Al-7%Si with approximate 0.5% by weight of TiH_2 as a foaming agent.

For characterization, the measurements of cell size of the porosity were done microscopically and evaluated [5] as $(ab)^{1/2}$, where a and b are major and minor axis. For each test sample, 20 point measurements were made at various locations.

Lastly, as above fabricated aluminum foam sample as well as prefabricated foamed sample using powder metallurgy (P/M) technique were cut with the laser μ-jet. It uses a pulsed Nd-YAG laser beam that is guided through a water jet of about 100 μm in diameter. Fig. 5A shows the sections of such laser cut sample. In the conventional cutting of aluminum foam with the laser, the cut section of the pores is severally damaged due to thermal effects. But when the laser beam is guided through the water jet, the thermal effects are greatly reduced and the cut cross-section of the pores as observed from the Fig. 5A-c become relatively better. It was also

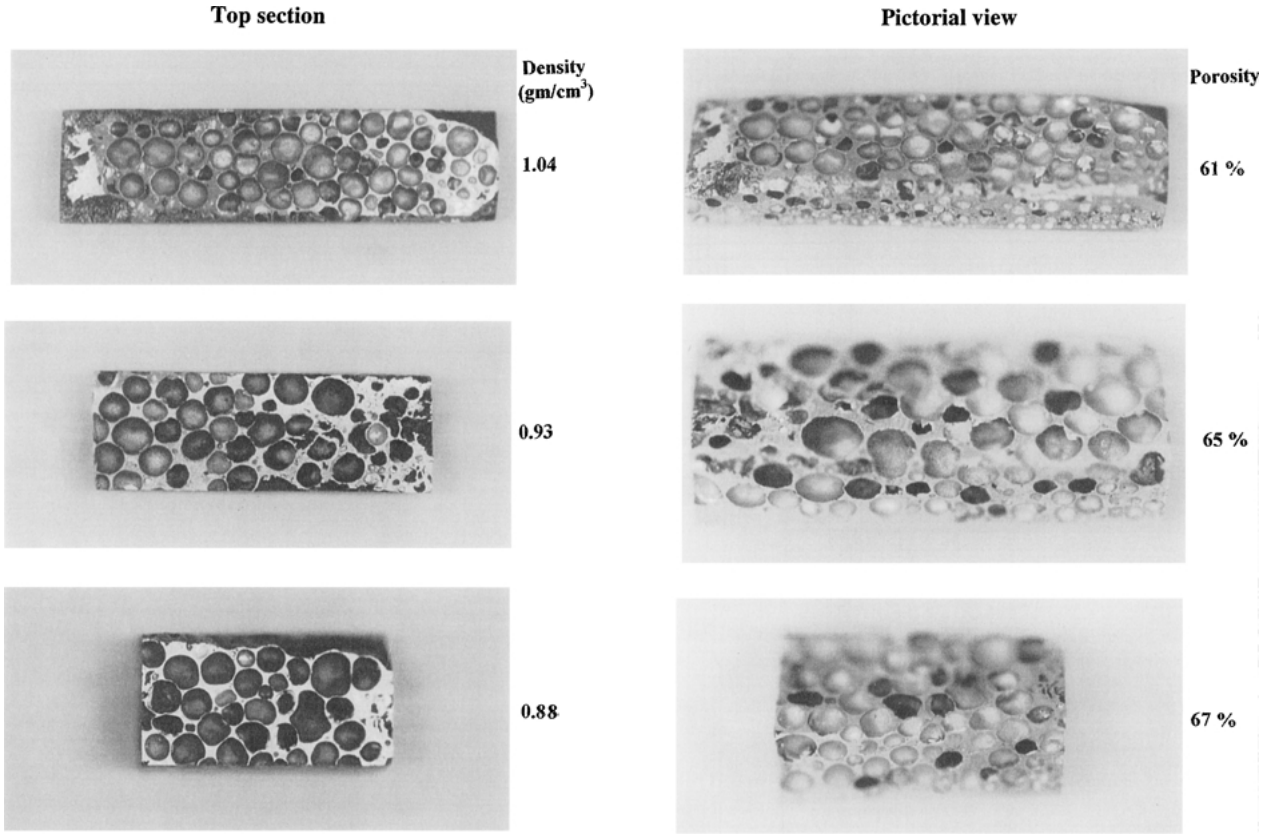

Figure 3 Top section and pictorial photographic view of Al-7%Si foam: (a) $\rho^* = 1.04$ gm/cm^3; porosity = 61%, (b) $\rho^* = 0.93$ gm/cm^3; porosity = 65%, and (c) $\rho^* = 0.88$ gm/cm^3; porosity = 67%.

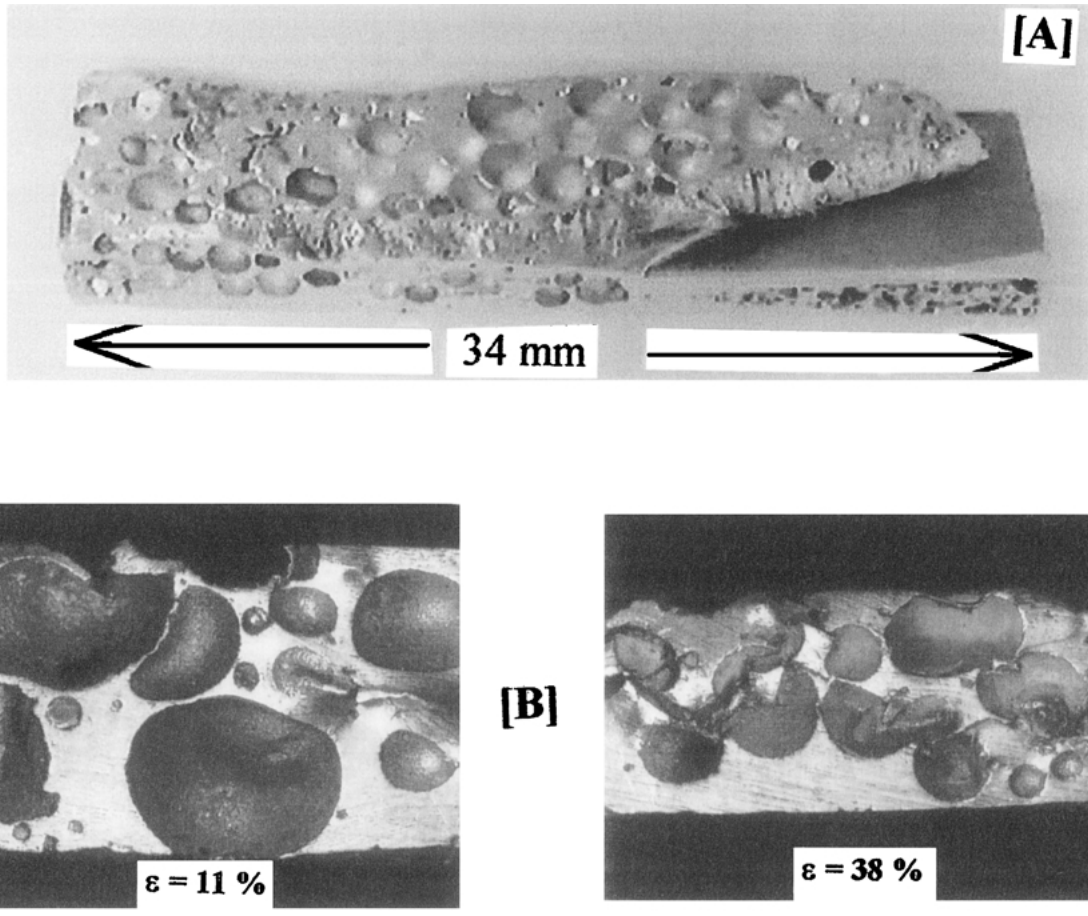

Figure 4 [A]: Photographic and pictorial view section of aluminum foamed sample. Laser: cw/pulse Nd-YAG. Processing parameters: $P_{avg} = 2$ kW; $P_{peak} = 4$ kW; $Ar = 50$ l/min; Processing speed (V) = 0.3 m/min; Duty cycle = 50%; Pulse repetition rate = 100 Hz. [B]: Deformation of the specimen during the compressive test.

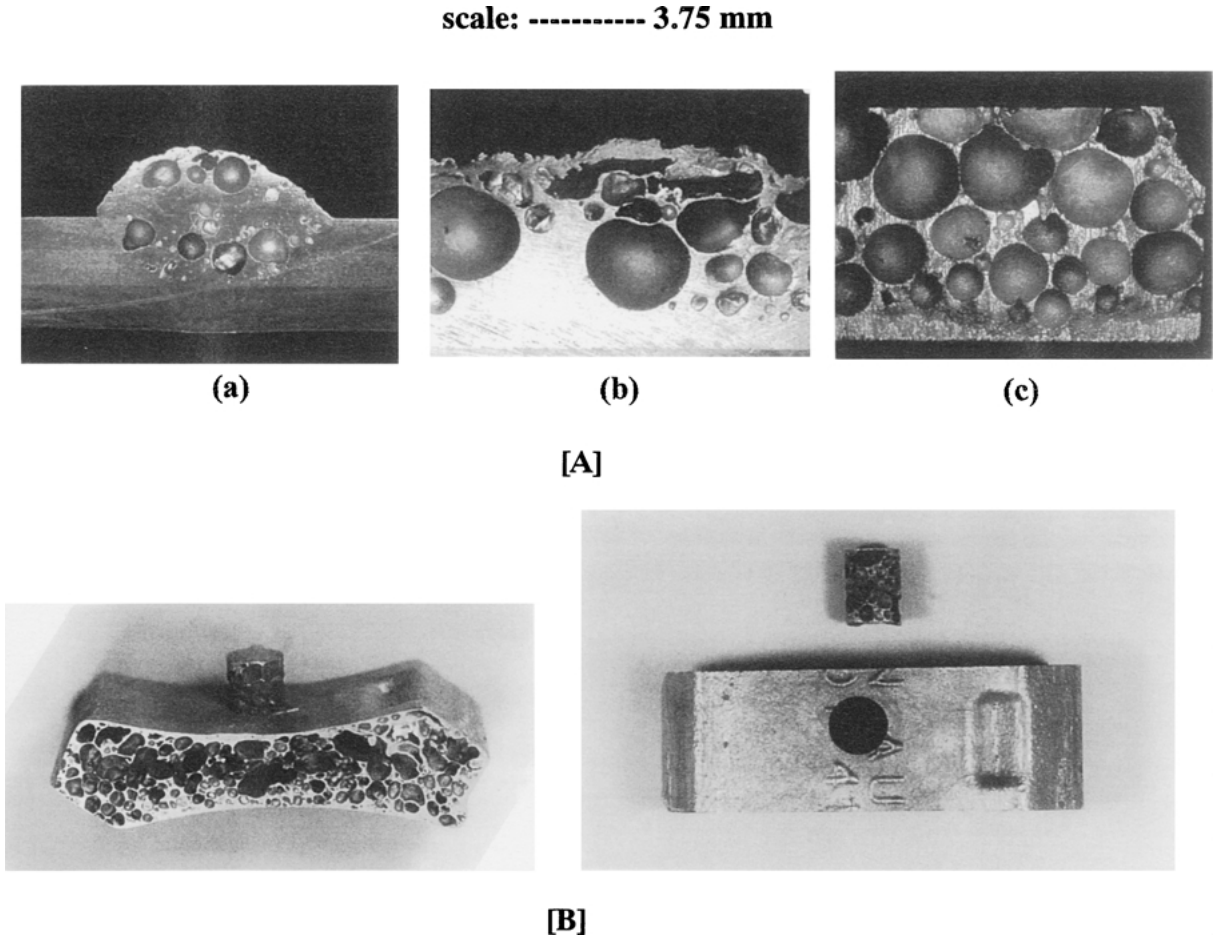

Figure 5 Laser μ-jet cut (A) vertical section of Al-7%Si foam for foaming temperature: (A-a) at melting point: under-foaming condition; (A-b) much above melting point: bad quality foam; (A-c) slightly above melting point: optimum quality foam. (B) Circular hole cut cross-section of an P/M-fabricated foam.

possible to cut the shaped hole in a near net-shape foamed structure (Fig. 5B).

4. Results and discussion

For the microscopic observation of the cell morphology, top and the side cross-section of the foamed Al-blocks were made by removing the oxide crest and then polishing with the conventional technique. Variation in the cell morphology was observed using an optical microscope. Figs. 1, 3, 4, 5 and 6 shows the side, pictorial and top view sections of the foam, which exhibits a closed cell structure. A strong variation in the cell size or structure can be seen depending upon the processing parameters and their shape varies from circular to irregular ellipsoidal or deformed circular structure. It can be explained by considering the beam interaction time ($t_{\text{int.}}$ = spot size/processing speed). On carefully examination of the Fig. 1B, one finds that initially the width of the unfoamed aluminum sandwich is 3.72 mm only. Upon laser irradiation it expands predominantly unidirectional in the direction of the laser beam. The expansion process in the other directions is relatively small and can be neglected. One find that at higher processing speed that is short beam interaction time (0.16 sec), the cell size is relatively fine ($\approx$0.2 mm) and the width of foamed structure already becomes 5.03 mm (Fig. 1B-a), but still the base has not fully expanded. On the other hand at lower processing speed that is long interaction time (0.86 sec), the width of foamed structure is scaled up to 8.13 mm (Fig. 1B-c) having a large size porosity and with a cell size of about 3 mm. Besides that the cell shape is also partially deformed from its primitive shape due to the gravitational effects on foam, which is playing against the pressure of the blowing agent that is exerting an internal force on the cells that is equal in all directions [8].

Furthermore, non-optimized processing conditions have severe effects on foaming process. Since TiH_2 absorbs heat when decomposing, therefore the actual melt temperature should be higher than the theoretical temperature [9]. As TiH_2 decomposition starts, the melt temperature drops down to the solidification temperature interval. Therefore, if the initial foaming temperature is 660°C it will put restrain on effective solidification temperature interval for foaming procedure. Thus the uniform distribution of the foaming agent is hindered. This is especially true in case of very fast processing speed that is short interaction time (Fig. 5A-a). On the other hand if the foaming temperature reaches high value then the foaming will advance above the temperature level for keeping the alloy as liquid. As the melt is with low viscosity and the bubbles are easy to aggregate to release, so that poor quality of foam is very likely (Fig. 5A-b). This post collapse of the pores or foam could be due to the superheat generated when

the beam interaction time [10] becomes considerably large. However, at the optimized processing conditions for the foaming temperature, the overall conditions are beneficial to TiH_2 decomposition and the melt foaming that is completed within the solid temperature interval. Microscopically, the cooling rate also varies substantially over the depth of the pool as the temperature gradient is lower at the surface and maximum at the bottom of the pool. Besides that due to a gradient of the molten liquid pressure, the bubble expands as it moves from bottom to the top surface. Therefore one also observes a systematic change in the porosity size from top to the bottom (Fig. 5A-c). Overall, foam density is decreasing with height i.e., as one move from bottom to the top. The drainage of the excess melt from the foam column into the underlying layer is driven by hydrostatics pressure and gravity pulling, which may cause the bubbles to become distorted. Interestingly, the melt collapse at the top of the surface resulting in closure of the pores, whereas the foam collapse at the bottom, since the film in the foam bubble are more susceptible to rupture by temperature gradient which is maximum at the bottom of the pool. Besides, that the diffusion of the gas can cause instability of the foam, in which case the gas is forced across the thin films from smaller bubbles into larger ones. This is due to the reason that the pressure inside a small bubble is greater than that in a large sized bubble, and the gas solubility increases with the pressure, therefore more gas dissolves near the small bubbles than the larger ones. Moreover, the solubility of hydrogen gas released from dissociation of TiH_2 is much higher in molten metal than in solid metal. This causes diffusion of the gas to occur across the walls, with smaller bubbles growing at the expanse of the large ones [22].

To study the deformation of the foam, the compressive tests were carried out with a foamed specimen (Fig. 4A) fabricated by using Nd-YAG laser. It was further cut into various blocks for compressive test under different loading conditions. The study was carried out at room temperature, with a displacement control at a strain rate of 1 mm/min. The deformation in each of the test pieces after the compressive test was photographed. The results are shown in Fig. 4B. It is observed that the deformation is predominantly near the top and propagates downwards with the increasing load.

TABLE IIa Density and strain of the Al-7%Si foam (CO_2-laser)

Test sample	(a)	(b)	(c)	(d)
Density (ρ^*) gm/cm^3	1.84	1.04	0.93	0.88
Relative density (ρ^*/ρ_s)	0.68	0.39	0.35	0.33
Porosity $[1-(\rho^*/\rho_s)]$	32%	61%	65%	67%
Densification strain $[1-1.4(\rho^*/\rho_s)]$	0.04	0.46	0.52	0.54
Microhardness (HV)	80	86	73	84

TABLE IIb Density and strain of the Al-7%Si foam (Nd-YAG laser)

Density (ρ^*) gm/cm^3	Relative density (ρ^*/ρ_s)	Porosity $[1-(\rho^*/\rho_s)]$	Densification strain $[1-1.4(\rho^*/\rho_s)]$	Hardness (HV)
1.08	0.40	60%	0.44	77

This is possibly due to the pore size gradient from top to bottom [10]. Besides this, deformation occurs mostly at weaker columns of the large size pores.

For further characterization, the density of each aluminum foam block was calculated from the measured weight and the volume. The volume of each foamed specimen was calculated from its dimensions. The density of the aluminum foamed blocks were measured to be $\rho^* = 1.84$, 1.04, 0.93 and 0.88 gm/cm^3. Taking into account the density of the pure aluminum ($\rho_s = 2.6989$ gm/cm^3), various other parameters, for example relative density, porosity and densification strain etc. were calculated [11, 12] and are summarized in Table IIa. To make an estimate of the cell wall yield strength, microhardness measurements were made on the cell edges that are at the cross-sectional area between the cells (Fig. 6b). A Matsuzawa (Model: MXT70) microhardness testing machine fitted with the Vickers indenter and using a 10 gm load was used for the entire test. Fig. 7 shows a plot of hardness versus density for the various foamed test samples. The microhardness averaged to be 81 HV. Also for the foam test sample generated with Nd-YAG laser, the foaming characteristics did not differ much. In this case the density of an aluminum foamed block was measured to be $\rho^* = 1.08$ gm/cm^3. Pore size, wall structure and the microhardness (77 HV) with porosity of 60%, were roughly in the same order (Table IIb). A rough

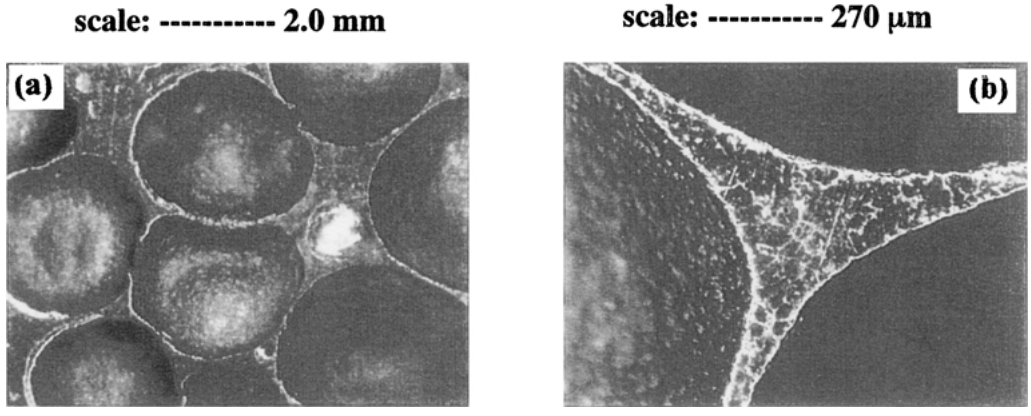

Figure 6 Optical photographs of the microstructure showing: (a) pores and (b) section between cell walls of Al-7%Si foam.

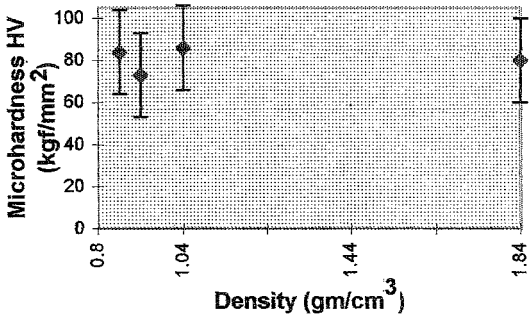

Figure 7 Microhardness versus density of Al-7%Si foam. Load = 10 g.

estimate of the cell wall yield strength was made from the microhardness measurement [5]. This amounts to be $\sigma_{ys} \cong$ HV/3, that corresponds to 265 MPa which is slightly higher than (250 MPa) already reported [5, 13]. This is possibly due to higher Si content, moreover in considering the three points close to the lower limiting value of 0.3 for relative density, which hold the above mentioned assumption of yield strength.

5. Conclusions

The main conclusions with the CO_2/Nd-YAG laser foaming can be summarized as follow:

1. There is a predominantly localized and unidirectional expansion of the foam in the direction of laser irradiation.
2. A pore size gradient does exist with the slow and fast processing speed as well as from top to bottom of the foamed sample.
3. The pores in the foamed structure are circular, irregular ellipsoidal or deformed circular and constitute closed cell structure.
4. Porous structures with a relative density of 0.33 were created.
5. Examples of laser assisted cutting of aluminum foam were also demonstrated.
6. It is also realised, that non-optimised parameters and unavoidable gravitational effects could have adverse effects on the foaming process.

However, there is a potential for substantial improvement in the process for foaming, if such defects could be reduced through an improved technique. Foams produced by this method may enlarge the application range of cellular materials such as graded porous structures and net-shaping. It shall further offer the possibility of basic investigations of many engineering problems.

Acknowledgement

The author expresses his gratitude to Prof. S. Sugiyama of Ritsumeikan University for his kind support.

References

1. C. PARK and S. R. NUTT, *Mater. Sci. Eng.* A **288** (2000) 111.
2. G. J. DAVIES and SHU ZHEN, *J. Mater. Sci.* **18** (1983) 1899.
3. J. BANHART and J. BAUMEISTER, *ibid.* **33** (1998) 1431.
4. J. BANHART, *Prog. in Mater. Sci.* **46** (2001) 559.
5. A. E. SIMONE and L. J. GIBSON, *Acta Mater.* **46** (1998) 3109.
6. Y. SUGIMURA, J. MEYER, M. Y. HE, H. BARTSMITH, J. GRENSTEDT and A. G. EVANS, *ibid.* **45** (1997) 5245.
7. K. BOOMSMA and D. POULIKAKOS, *Intl. J. Heat and Mass Transfer* **44** (2001) 827.
8. S. P. McMANUS, *Polym. Preprints* **41** (2000) 1056.
9. SHAOJUN CHU, QUIANG NIU, YIXIAN LIN and KENG WU, *ISIJ International* **40** (2000) 597.
10. Y. P. KATHURIA, *Mater. Sci. Technol.* **17** (2001) 593.
11. L. J. GIBSON and M. F. ASHBY (eds.), "Cellular Solids: Structure and Properties," 2nd ed. (Cambridge University Press, Cambridge, UK, 1997).
12. K. Y. G. McCULLOUGH, N. A. FLECK and M. F. ASHBY, *Acta Mater.* **8** (1999) 2323.
13. E. ANDREWS, W. SANDERS and L. J. GIBSON, *Mater. Sci. Eng.* A **270** (1999) 113.
14. P. H. THORNTON and C. L. MAGEE, *Metall. Trans.* **6A** (1975) 1253.
15. D. WEARE and M. A. FORTES, *Advan. in Phys.* **43** (1994) 685.
16. T. G. NIEH, J. H. KINNEY and J. WADSWORTH, *Scripta Mater.* **38** (1998) 1487.
17. H. FUSHENG and Z. ZHENGANG, *J. Mater. Sci.* **31** (1999) 291.
18. Z. X. GUO, C. S. Y. JEE, N. OEZGUEVEN and J. R. G. EVANS, *Mater. Sci. and Technol.* **16** (2000) 776.
19. C. KOERNE, F. BERGER, M. ARNOLD, C. STADELMANN and R. F. SINGER, *Mater. Sci. and Technol.* **16** (2000) 781.
20. Y. P. KATHURIA, in Proc. Instn. Mech. Engrs. Part B: J. Eng. Manufac. **217** (2003) 193.
21. *Idem.*, *Advan. Eng. Mater.* **3** (2001) 702.
22. R. J. PUGH, in "Handbook of Applied Surface and Colloid Chemistry," Vol. 2, edited by K. Holmberg (John Willey Pub., 2001) Chap. 2, p. 23.
23. K. A. DANNEMANN and J. LANKFORD JR., *Mater. Sci. Eng.* A **293** (2000) 157.
24. C. MOTZ and R. PIPPAN, *Acta Mater.* **49** (2001) 2463.
25. T. J. LU and J. M. ONG, *J. Mater. Sci.* **36** (2001) 2773.
26. B. KRISZT, M. FOUROUGHI, K. FAURE and H. P. DEGISCHER, *Mater. Sci. Technol.* **16** (2000) 792.
27. C. S. Y. JEE, N. OZGUVEN, Z. X. GUO and J. R. G. EVANS, *Metall. Trans.* **31B** (2000) 1345.

Received 9 August 2002
and accepted 3 April 2003